

# RIPK1 and CCL5 in Multiple Sclerosis

A thesis submitted by

Jiya Hao

In Partial fulfillment of the requirements for the degree of

Master of Science

in

Pharmacology and Drug Development

Tufts University

Graduate School of Biomedical Sciences

May 2023

Advisor: Alexei Degterev, Ph.D.

## Abstract

Receptor interacting protein kinase 1 (RIPK1) regulates cell death by inducing caspase-8-dependent apoptosis and RIPK3 and mixed lineage kinase like (MLKL)-dependent necroptosis, and as its ability to mediate cell death and inflammatory signaling, RIPK1 is becoming a promising therapeutic target for a wide range of human neurodegenerative, autoimmune, and inflammatory diseases, including multiple sclerosis. Previous studies demonstrated that RIPK1 inhibitor attenuated the disease progression in experimental autoimmune encephalomyelitis (EAE) mouse model, which is the most commonly used experimental model for the human multiple sclerosis. However, the underlying mechanism is unclear. Prior work in our lab observed that C–C chemokine ligand 5 (CCL5) decreased in RIPK1 inhibitor GSK treated EAE mice spinal cord compared with the vehicle (without drug). Here, we investigate which kind of cell express CCL5 in EAE mice spinal cord and where do these cells locate, expecting this would enlighten us on the mechanism of RIPK1 inhibitor GSK. Therefore, in this paper we collected spinal cord from EAE mice treated with different conditions: vehicle, GSK, score1 and control, and cut slides to stain. In the whole experiment, depending on different antibodies, two staining methods were performed: 1) Immunohistochemistry (Frozen Sections); and 2) Multiplex Immunohistochemistry. By co-staining with different antibodies, we find that the level of CCR5 and CXCR3, which are the receptor of CCL5 and CXCL10, is higher in vehicle group compared with GSK and score1, confirming our previous result and also showing that RIP1 inhibitor protects spinal cord and prevents the disease progression. In the meantime, we demonstrate that CCR5 and CXCR3 signal are outside cells in lesions and greatly reduce in uninjured area. Further, we uncover

that it is macrophage in lesions that expresses CCL5, while in uninjured area, CCL5 is produced by both microglia and astrocytes.

## Dedication

I wholeheartedly dedicate this work to my beloved parents and brother who encouraged me to pursue science and continuously supported me spiritually, emotionally and financially.

To my advisor, Dr. Degterev, who conveyed a spirit of adventure in regard to research and was the guiding light every step of the way as I researched for this thesis.

## Acknowledgments

Advisor: Alexei Degterev

Thesis reader: Yongjie Yang

Cell, Molecular & Developmental Biology

Aislinn Keane, Nathan Brackins, Benjamin Undurraga, Rachel Covitz for their  
patience and support.

## Table of Contents

Title page.....	i
Abstract.....	ii
Dedication.....	iv
Acknowledgments.....	v
Table of Contents.....	vi
List of figures .....	viii
List of Abbreviations.....	ix
Chapter 1: Introduction.....	1
1.1 Necroptosis and RIPK1.....	1
1.2. Immunopathogenesis of MS.....	2
1.3. RIPK1 and CCL5 in MS.....	4
Chapter 2: Materials and Methods.....	6
2.1. EAE Mice Spinal Cord Slides Preparation.....	6
2.2. Antibodies.....	6
2.3. Reagents.....	7
2.4. Immunohistochemistry (Frozen Sections).....	8
2.5. Multiplex Immunohistochemistry.....	9
2.6. Image Taking.....	11
2.7. Statistical analysis.....	11
2.8. Collaboration.....	12
Chapter 3: Results.....	13
3.1. Verification of CCR5 and CXCR3 signal change in vehicle-GSK-score1- control EAE mice.....	13
3.2. CCR5 and CXCR3 signal are outside nucleus in lesion and greatly reduce in uninjured area.....	16
3.3. Majority of the cells in lesion are macrophage, and in uninjured area are microglia.....	17
3.4. Both macrophage and microglia produce CCL5.....	20
3.5. Collaboration.....	21
Chapter 4: Discussion.....	22
4.1. RIPK1 inhibitor affects the recruitment of CCR5+ and CXCR3+ cells to lesion.....	22
4.2. Cell composition in EAE spinal cord.....	23
4.3. limitations and Further studies.....	24
Chapter 5: Appendix.....	25

Chapter 6: Bibliography.....26

## List of Figures

Figure3.1: CD11b + CCR5 signal was highest in vehicle and decreased in GSK, score1 and control.....	14
Figure3.2: CD11b + CXCR3 signal showed the highest in vehicle and redeced in GSK, score1 and control.....	15
Figure3.3: High magnification images of CCR5, CXCR3 and CCL5 in lesion and uninjured area. ....	17
Figure3.4: Most of cells in lesion are CD45 and Iba-1 double positive cells, whereas in uninjured area few of CD45 and Iba-1co-located. ....	18
Figure3.5: CD45 and CCL5 double positive make up the majority of cells in lesion, while in uninjured area there is almost none of double positive cells.....	19
Figure3.6: All the Iba-1 cells were CCL5 positive in lesions, while in uninjured area a few Iba-1 cells did not secret CCL5.....	20

## List of Abbreviations

ALS	Amyotrophic lateral sclerosis
APCs	Antigen-presenting cells
BBB	Blood–brain barrier
CCL5	C–C chemokine ligand 5
DD	Death domain
EAE	Experimental autoimmune encephalomyelitis
GFAP	Glial fibrillary acidic protein
GPCRs	G-protein coupled receptors
MHC	Major histocompatibility complex
MLKL	Mixed lineage kinase domain-like protein
MS	Multiple sclerosis
NF- $\kappa$ b	Nuclear factor $\kappa$ -light-chain-enhancer of activated B cells
OLs	Oligodendrocytes
RANTES	Regulated upon Activation Normal T cell Expressed and Secreted
RIPK1	Receptor-interacting serine/threonine-protein kinase 1
RIPK3	Receptor-interacting serine/threonine-protein kinase 3
TLR	Toll-like receptors
TNF	Tumor necrosis factor.
TNFR	Tumor necrosis factor receptor
TRADD	TNFR1-associated death domain protein

## Chapter 1: Introduction

### 1.1 Necroptosis and RIPK1

There are two different regulated cell death mechanisms: apoptosis and necroptosis. Necroptosis can be triggered when apoptosis is deficient. When the intracellular apoptotic signaling is absent, the necroptosis pathway would be activated, even though the extrinsic apoptosis pathway is triggered when Fas/TNFR receptor is stimulated (Degterev, Huang et al. 2005). In last decade, an abundance of studies and research about necroptosis revealed that necroptosis played an important role in several neurodegenerative diseases, including multiple sclerosis, Parkinson's disease and Alzheimer's disease (Yuan, Amin et al. 2019). RIPK1 kinase inhibitors have developed into early clinical trials for evaluation in inflammatory diseases including psoriasis, ulcerative colitis and neurological diseases such as amyotrophic lateral sclerosis (ALS) and Alzheimer's disease (Harris, Faucher et al. 2019). Prior study demonstrated that RIPK1, RIPK3 and MLKL were activated in cortical lesions from MS brain specimen, and also RIPK1 was elevated in the oligodendrocytes (OLs), microglia and neurons from corpus callosum both in a cuprizone model as well as in an EAE model of MS (Ofengeim, Ito et al. 2015). In addition, tumor necrosis factor (TNF) can damage OLs in MS with necrotic pathology by initiating the process of necroptosis (Dulamea 2017). OLs wrap nerve fibres in the CNS with layers of specialized cell membrane to form myelin sheaths, and demyelination in the CNS leads to neurodegeneration in MS (Jakel, Agirre et al. 2019, Yeung, Djelloul et al. 2019).

TNF, which is one of the most extensively studied neuroinflammatory cytokines, can interact with two receptors: TNFR1 and TNFR2. TNFR1 was expressed most

prominently in microglia and at a lower level in astrocytes, while TNFR2 expression was highly enriched only in microglia(Srinivasan, Friedman et al. 2016). Then because of the stimulation of TNFR1 by TNF, a large receptor-bound signaling complex, Complex I ((also known as TNF-receptor signalling complex,) is assembled through the recruitment of DD-containing proteins, RIPK1 and TNFR1-associated DD protein (TRADD) (Degterev, Ofengeim et al. 2019). Interaction between TNF and TNFR2 can not lead to the TNF-receptor signalling complex formation as TNFR2 is lack of the intracellular DD. Among multiple modifications that regulate RIPK1, ubiquitination is one of the most critical regulatory mechanisms. In complex I, RIPK1 is subject to several types of ubiquitin modifications, including M1, K11, K48 and K63 ubiquitylation, and which are important in the activation of RIPK1(Yuan, Amin et al. 2019). When apoptotic mediator caspase-8 activity is compromised, RIPK1 recruits and phosphorylates RIPK3, and the RIPK1/RIPK3 complex recruits and phosphorylates MLKL, thus forming the necrosome complex (Bertheloot, Latz et al. 2021). Eventually RIPK3 and MLKL are phosphorylated, and lead to disruption of the cellular membrane and execute necroptosis(Shan, Pan et al. 2018, Yu, Jiang et al. 2021). Therefore, as RIPK1 plays a key role in regulating the deleterious reaction downstream of TNFR1, and also its unique hydrophobic pocket in the allosteric regulatory domain enabled the development of highly selective small- molecule inhibitors of its kinase activity, targeting RIPK1 may help to inhibit multiple cell death pathways and ameliorate neuroinflammation (Mifflin, Ofengeim et al. 2020).

## 1.2. Immunopathogenesis of MS

Multiple sclerosis (MS) is a chronic central nervous system inflammatory disease, which focal lymphocytic infiltration leads to damage of myelin and axons(Compston

and Coles 2008). It is a complex and poorly understood condition. The cause of multiple sclerosis remains unclear, but current evidence indicates that it is environmental stimulus and genetic factors that lead to this autoimmune disorder in the central nervous system(Nicholas and Rashid 2013, Dobson and Giovannoni 2019). EAE is commonly employed as an experimental model for the human multiple sclerosis (MS) as it shares similar important features with MS. EAE has been a powerful tool for studying disease pathogenesis as well as potential therapeutic interventions(Constantinescu, Farooqi et al. 2011, Robinson, Harp et al. 2014).

The immunopathogenesis of MS is thought to result from the damage of self-tolerance to myelin and other CNS antigens, leading to consistent peripheral activation of autoreactive T cell. Previous study showed that the genes that influence T cell maturation are over expressed in multiple sclerosis, suggesting that immune dysregulation is involved in the critical mechanisms(International Multiple Sclerosis Genetics, Wellcome Trust Case Control et al. 2011), and also more evidence shows that B cells and cells from innate immune system play an important role(Yamout and Alroughani 2018).

Once activated in the periphery, myelin-reactive T cells are able to migrate across the blood–brain barrier (BBB). In CNS, the autoreactive peripherally activated T cells may become reactivated by antigen-presenting cells (APCs) presenting CNS autoantigens on major histocompatibility complex class II molecules (MHC) to the invading T cells (Selter and Hemmer 2013). Then an inflammatory cascade is triggered, resulting in the of cytokines and chemokines, recruitment of additional inflammatory cells including T cells, monocytes, and B cells and persistent activation of microglia and macrophages, all of which lead to myelin damage(Garg and Smith 2015).

Microglia and macrophages are the major cell types in MS lesions. Upon sensing tissue damage or pathogenic infiltrations in CNS, microglia become reactive. Reactive microglia and macrophages produce inflammatory cytokines such as TNF- $\alpha$ , interleukin (IL)-6, IL-1 $\beta$ , and IL-23 that leads to further immune activation(Kamma, Lasisi et al. 2022). And under certain circumstances, microglia and macrophages release excessive amounts of glutamate, which activates glutamate receptors, leading to influx of calcium through ion channels and cause necrotic damage to oligodendrocytes and axons(Inglese 2006). Astrocyte is also a cell type which is critically involved in the formation of lesions in MS white matter. They express toll-like receptors (TLR) and major histocompatibility complex class I and II. In addition, astrocytes regulate blood brain barrier (BBB) permeability and in modulate T cell activity through the production of cytokines(Ponath, Lincoln et al. 2018, Guerrero-Garcia 2020).

### 1.3. RIPK1 and CCL5 in MS

As tumor necrosis factor alpha (TNF $\alpha$ ) is a major cytokine that participates in multiple sclerosis (Pegoretti, Baron et al. 2018), and the activation of RIPK1 kinase in microglia and astrocytes induces a harmful neuroinflammatory process that contributes to the neurodegenerative environment of progressive MS(Zelic, Pontarelli et al. 2021), RIPK1- itself or as the downstream mediator of TNF- becomes a promising therapeutic target. A previous study already showed that RIP1 kinase inhibitor attenuated disease progression in the mouse experimental autoimmune encephalomyelitis (EAE) model which is the most commonly used experimental model for the human multiple sclerosis(MS) (Yoshikawa, Saitoh et al. 2018), and blocking the activity of RIP1 kinase can eliminate the microglial necrosis induced by

TLR activation(Kim and Li 2013), and protect against oligodendrocyte cell death (Ofengeim, Ito et al. 2015). The beneficial effects of RIPK1 inhibition may be attributed to modulation of inflammation and inhibition of necrosis in susceptible oligodendrocytes and neurons(Degterev, Ofengeim et al. 2019).

The cytokine CCL5 (C-C motif chemokine 5), which has been initially termed RANTES (Regulated upon Activation Normal T cell Expressed and Secreted), is a potent chemokine(Kranjc, Novak et al. 2019). Chemokines belong to the superfamily of chemotactic cytokines, whose receptors are typically G-protein coupled receptors (GPCRs). The CC chemokines are closely related to inflammation and the immune response. As a member of the CC subfamily, CCL5 is expressed in T lymphocytes, macrophages, selected tumor cells(Huang, Guo et al. 2021, Hinrichs, Blokland et al. 2022).

CCL5 is a target gene of NF- $\kappa$ B activity, its production can be induced when NF- $\kappa$ B is activated by a wide variety of stimuli including CD40L, IL-15, TNF- $\alpha$  and LPS (Lawrence 2009, Aldinucci and Colombatti 2014). In addition, as RIPK1 serves as a main switch to control whether the cell undergoes NF- $\kappa$ B dependent inflammation, caspase-dependent apoptosis, or necroptosis in response to extracellular stimuli(Karunakaran, Nguyen et al. 2021), probably that is why GSK is able to down regulate CCL5 in EAE mouse model.

## Chapter 2: Materials and Methods

### 2.1. EAE Mice Spinal Cord Slides Preparation

The whole experiment used mice spinal cord slides. All mice were female, and between 6-10 weeks when EAE was induced. One set of mice without any treatment as control and three sets of mice were induced EAE at the same time and around 14 days after EAE was induced, when they reached a score of one, the spinal cord samples of one set were collected, and the other two sets of mice were treated for three days with either vehicle or GSK. The vehicle mice developed to score 3-3.5 or even higher while GSK mice stopped disease progressing and stayed around 1-1.5 as GSK protected the mice. After spinal cords were collected from these four sets of mice, the samples were fixed by 4% PFA for 5 minutes, then embedded with OTC and stored in -80°C fridge.

To prepare slides for experiment, the spinal cord samples were cut at 20 nm thickness on Cryostat, and frozen at -80°C overnight. On each slide we had multiple 20nm cross-sections of spinal cord, so that we had enough number of samples for the statistical analysis.

### 2.2. Antibodies

The following primary antibodies acquired from ABclonal Technology were used: AIF1/IBA1 Rabbit pAb (A1527), CXCR3 Rabbit pAb (A2939), CCL5/RANTES Rabbit pAb (A14192), and CCR5 Rabbit pAb (A20261). Two antibodies from BD Pharmingen were used: Purified Rat Anti-CD11b (550282), Purified Rat Anti-Mouse CD45 (550539). Anti Iba-1 Rabbit for Immunocytochemistry (019-19741) was bought

from FUJIFILM Wako Pure Chemical Corporation. Polyclonal Rabbit Anti-Glial Fibrillary Acidic Protein (Z033401-2) was bought from Agilent DaKo.

The two secondary antibodies from Cell Signaling Technology were used: Anti-rabbit IgG (H+L) F(ab')<sub>2</sub> Fragment Alexa Fluor® 647 Conjugate (4414), Anti-mouse IgG (H+L), F(ab')<sub>2</sub> Fragment Alexa Fluor® 594 Conjugate (8890).

Other two secondary antibodies from ThermoFisher Scientific were used: Goat anti-Rat IgG (H+L) Cross-Adsorbed Secondary Antibody Alexa Fluor™ 568 (A11077), Goat anti-Mouse IgG (H+L) Highly Cross-Adsorbed Secondary Antibody Alexa Fluor™ 568 (A11031).

### 2.3. Reagents

Normal Goat Serum (Southern Biotech, 0060-01), Hoechst 33342, Trihydrochloride, Trihydrate - 10 mg/mL Solution in Water (ThermoFisher Scientific, H3570), Hydrogen Peroxide 30% (Certified ACS) (Thermo Scientific, BP2633500), Xylenes (Histological) (Thermo Scientific, X3RB50), Formaldehyde, 16%, methanol free, Ultra Pure (Polyscience, 18814-10), ProLong™ Gold Antifade Mountant (ThermoFisher Scientific, P36930), Triton X-100 (ThermoFisher Scientific, A16046-AP), IHC-Tek™ Epitope Retrieval Solution (IHC World, IW-1100), Ethanol 200 Proof (Decon Labs, 2701).

And for multiplex immunohistochemistry, we bought Opal™ 4-Color Manual IHC Kit from Akoya Biosciences (NEL820001KT). The reagents we used in the kit included: reactive fluorophores Opal 570 (FP1488001KT) and Opal 690 (FP1497001KT), 10X Spectral DAPI (FP1490), 1X Plus Manual Amplification Diluent, 1X Antibody Diluent/Block, 1X Opal Anti-Ms + Rb HRP, DMSO.

## 2.4. Immunohistochemistry (Frozen Sections)

This method was used when only one primary antibody is needed in staining, or primary antibodies are raised in the different host species.

After the EAE mice spinal cord slides were frozen at  $-80^{\circ}\text{C}$  fridge overnight, took slides out and let slides thaw and dry completely at room temperature. To fix the slides, put the slides in ethanol at  $-20^{\circ}\text{C}$  for 10 minutes, then let slides dry again at room temperature.

The hydrophobic barrier pen (EMD Millipore, 402176-1EA) was used to completely surround the tissue section on the slide. Tissue sections were covered with PBS and slides were incubated for 10 minutes to re-hydrate, then washed and repeated PBS incubation. The buffer was dumped on paper towel directly (same as the following steps). Then slides were incubated in Permeabilization Buffer (1% normal goat serum and 0.4% Triton x-100 in PBS) for 10 minutes twice, and applied Blocking Buffer (5% goat serum and 0.4% Triton x-100 in PBS) to cover tissue sections for 30 minutes. Before draining off the blocking buffer, primary antibodies were diluted in permeabilization buffer (CD45 1:50, CD11b 1:100, Iba-1 1:250, GFAP 1:100, CCL5 1:200, CCR5 1:200, CXCR3 1:100). After applying enough volume of primary antibody solution to cover the spinal cord section, the slides were incubated in a humidified chamber at  $4^{\circ}\text{C}$  overnight.

On the next day, primary antibody solution was removed from slides and tissue sections were washed with permeabilization buffer 10 minutes three times. After secondary antibodies were diluted (1:2000 in permeabilization buffer) and centrifuged at 14000rpm for 2 minutes, sections were covered with secondary antibody solution and incubated for two hours in dark at room temperature. After secondary antibody

solution was drained off, slides were washed with permeabilization buffer 10 min three times. Then the slides were counter-stained with Hoescht (1:1000 in PBS) 30 minutes in dark, and washed with PBS 10 min three times.

Before cover slips were applied, excess buffer was tapped off or blotted with paper towels, then the ProLong Gold Antifade Mountant media was added to slides, usually 20  $\mu$ l is enough for six sections. The edges of coverslips were sealed with nail polish when the slides were cured.

## 2.5. Multiplex Immunohistochemistry

This method allows staining of multiple IHC targets using unlabeled primary antibodies raised in the same species, which can effectively avoid the secondary species-specific antibodies cross-react with the primary antibodies.

The slides first were dry and fixed by ethanol same as mentioned in Immunohistochemistry (Frozen Sections). Then the slides were placed in a processing jar, and 16% PFA was diluted to 4%, and filled the jar with the 4% PFA solution. After 20 minutes treatment with 4% PFA, the slides were washed with PBS twice, each time 10 minutes. Then the slides were incubated in different dilutions of ethanol (80%EtOH, 90 % EtOH, 100% EtOH, 100% EtOH), 10 minutes for each dilution. After draining off ethanol, xylene was added to the processing jar and incubated slides with xylene 5 minutes three times. This process was done in chemical fume hood. Then the slides were incubated in different dilutions of ethanol but opposite sequence (100%EtOH, 100%EtOH, 90%EtOH, 80%EtOH), and then washed with distilled water. Subsequently, slides were permeated with 0.1% Tween20 in PBS for 10 minutes and washed with PBS twice. After that the processing jar was filled with epitope retrieval solution to cover the slides and placed in retrieval steamer for 40 minutes. After the

processing jar cooled down to RT for at least 15 minutes, the slides were washed with 1×TBST.

The slides were taken out from processing jar and placed in a humidified chamber, the hydrophobic barrier pen was used to surround the tissue section on the slide. The slides were not dry during this process. After slides were incubated with PBS 10 minutes twice and followed by Permeabilization Buffer (1% normal goat serum 0.4% Triton x-100 in PBS) 10 minutes twice, tissue sections were covered with 1X Antibody Diluent/Block buffer and incubated for 10 minutes at room temperature. Primary antibody was diluted in 1X Antibody Diluent/Block buffer (same dilution mentioned in Immunohistochemistry Frozen Sections), and added to cover all the spinal cord sections. The slides were incubated in the humidified chamber at 4°C overnight.

On the second day, after the slides were washed with TBST for 2 minutes, 3 times at room temperature, 1X Opal Anti-Ms + Rb HRP was applied, and slides were incubated in Polymer HRP Ms + Rb for 10 minutes at room temperature. Then the tissue sections were washed with TBST 3 x 2 minutes preferably with agitation. To make Opal Fluorophore 570 Working Solution, Opal Fluorophore 570 was reconstituted in 75 µl of DMSO, and Opal Fluorophore 570 was diluted in 1X Plus Manual Amplification Diluent (1:100), then 100-300 µL of Opal Fluorophore Working Solution was pipetted onto each slide. After incubated with Opal Fluorophore Working Solution 570 10 minutes, the slides were rinsed in TBST 3 x 2 minutes. To strip the primary-secondary-HRP complex allowing introduction of the next primary antibody, the slides were placed in processing jar which was filled with the appropriate IHC-Tek™ Epitope Retrieval Solution. The processing jar was put in 95 °C water bath 20 minutes, then slides cooled down on ice before proceeding (15-30

minutes). After slides were rinsed in distilled water followed by TBST, 1X Antibody Diluent/Block buffer was applied again for 10 minutes, and then the second primary antibody was diluted and pipetted onto slides. The slides were incubated in the humidified chamber at 4°C overnight.

On the third day, introduction of 1X Opal Anti-Ms + Rb HRP step was repeated, then the slides were incubated with Opal Fluorophore 690 working solution 10 minutes. Two drops of 10X Spectral DAPI was added into 1ml of TBST, and DAPI Working Solution was applied for 5 minutes in a humidity chamber. After the slides were washed for 2 min in TBST buffer and then for 2 min in water, coverslip slides with ProLong Gold Antifade Mountant media. The edges of coverslips were sealed with nail polish when the slides were cured.

## 2.6. Image Taking.

The 60x magnification images of spinal cord sections were taken by Nikon AR1 and Leica SP8 confocal microscopy, the lower resolution 20x images were taken by Keyence microscopy.

## 2.7. Statistical analysis

All the figures were analyzed on image J. The lesion area and signal intensity were measured by ROI manger (Figure 3.1, Figure 3.2). Cell counting were performed by plugins-analyze-cell counter, this function can also make markers of different color on different cell types which was helpful to identify whether the cells were double positive (Figure 3.4, Figure 3.5, Figure 3.6).

All data are shown as mean  $\pm$  standard error. Two-tailed unpaired Student's t test were used for comparisons. Statistical analyses were performed using GraphPad

Prism. All data shown represent the results obtained from independent experiments.

Values of  $P < 0.05$  were considered statistically significant. In the figures, \* $P < 0.05$ ,

\*\* $P < 0.01$ , and \*\*\* $P < 0.001$ .

## 2.8. Collaboration

The induction of EAE on mice and all the spinal cord samples of EAE mice used in experiment were finished, collected, fixed and embedded by Aislinn Keane, and other methods were performed by Jiya Hao.

## Chapter 3: Results

### 3.1. Verification of CCR5 and CXCR3 signal change in vehicle-GSK-score1-control EAE mice

As the EAE mice model was set up as described in Methods (2.1), we got four sets of EAE mice spinal cord samples: vehicle (score 3-3.5 or higher), GSK (score 1-1.5), score 1 and control. A prior study in our lab indicated that CCL5 decreased in GSK compared with vehicle group, and also the data we got in flow cytometry showed that CD11b<sup>+</sup> CCR5<sup>+</sup> and CD11b<sup>+</sup> CXCR3<sup>+</sup> cells gradually reduced in vehicle-GSK-score 1-control spinal cord samples. Therefore, it seems possible to figure out the underlying mechanism about how RIPK1 inhibitor GSK prevents disease progression through analyzing CCL5 production in EAE mouse model.

First of all, to confirm the abovementioned results experimentally for sure, two sets of vehicle, GSK, score 1 and control spinal cord slides were stained with CCR5 and CD11b, CXCR3 and CD11b respectively. After the staining, we took image of three sections of each spinal cord slides with same magnification and exposure, then counted lesion number, measured the lesion area and signal intensity on Image J. On the slides we had multiple 20nm cross-sections of spinal cord, and the lesion sites, where many cells were clustered together, usually appeared on the rim of spinal cord section and located on the edge of white matter (Figure 3.1A, Figure 3.2A). Uninjured area is the area other than lesion in both white or grey matter, but the images of uninjured area in this paper were taken at the sites near lesions.

In CD11b and CCR5 co-staining, the lesion number reduced from vehicle to GSK, score 1 and control. Lesion area presented the same trend as lesion number, vehicle mice spinal cords had the highest lesion area. And the signal intensity did not

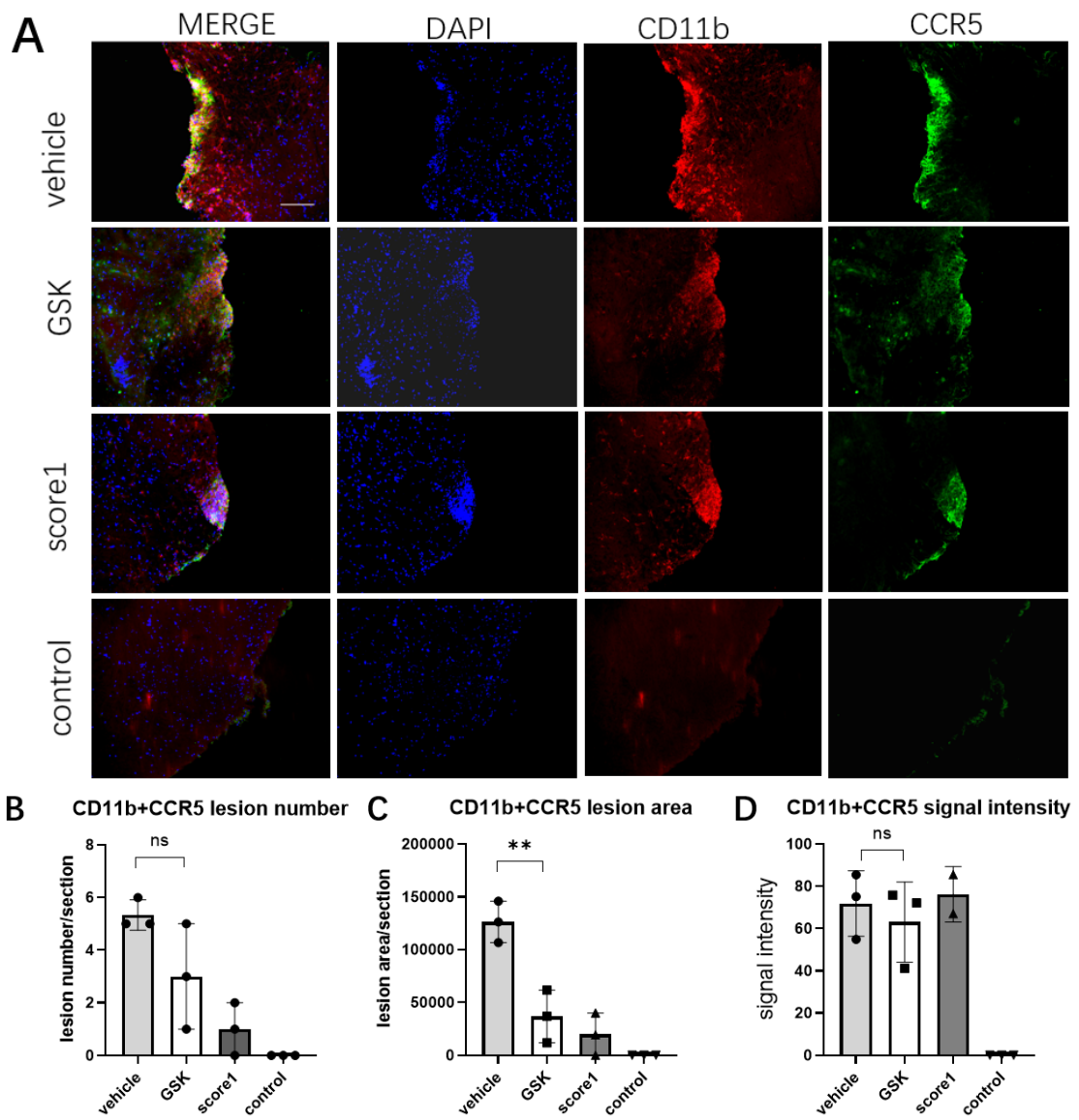


Figure 3.1: CD11b+CCR5 signal was highest in vehicle and decreased in GSK, score1 and control (scale bar=100  $\mu$ m). (A) Spinal cord slides were stained with CD11b, CCR5 and DAPI. The 20x images of lesion sites were analyzed by Keyence microscopy. Quantification of lesions in vehicle, GSK, score1 and control are shown in (B-D). (B) Lesion number of each spinal cord section. (C) Lesion area of each spinal cord section. (D) Signal intensity of the lesion sites. Data were analyzed by student's t-test and are expressed as mean  $\pm$  standard error.

show significant difference between vehicle, GSK and score1 groups (signal intensity: vehicle=71.83 $\pm$ 8.99 vs. GSK=63.03 $\pm$ 10.98,  $P > 0.05$ ) (Figure 3.1B-D). Though the data of lesion number was not significant different between vehicle and GSK (lesion number: vehicle=5.33 $\pm$ 0.33 vs. GSK=3.00 $\pm$ 1.15,  $P > 0.05$ ), we thought RIPK1 inhibitor GSK was protecting the EAE mice, because even very small lesions were

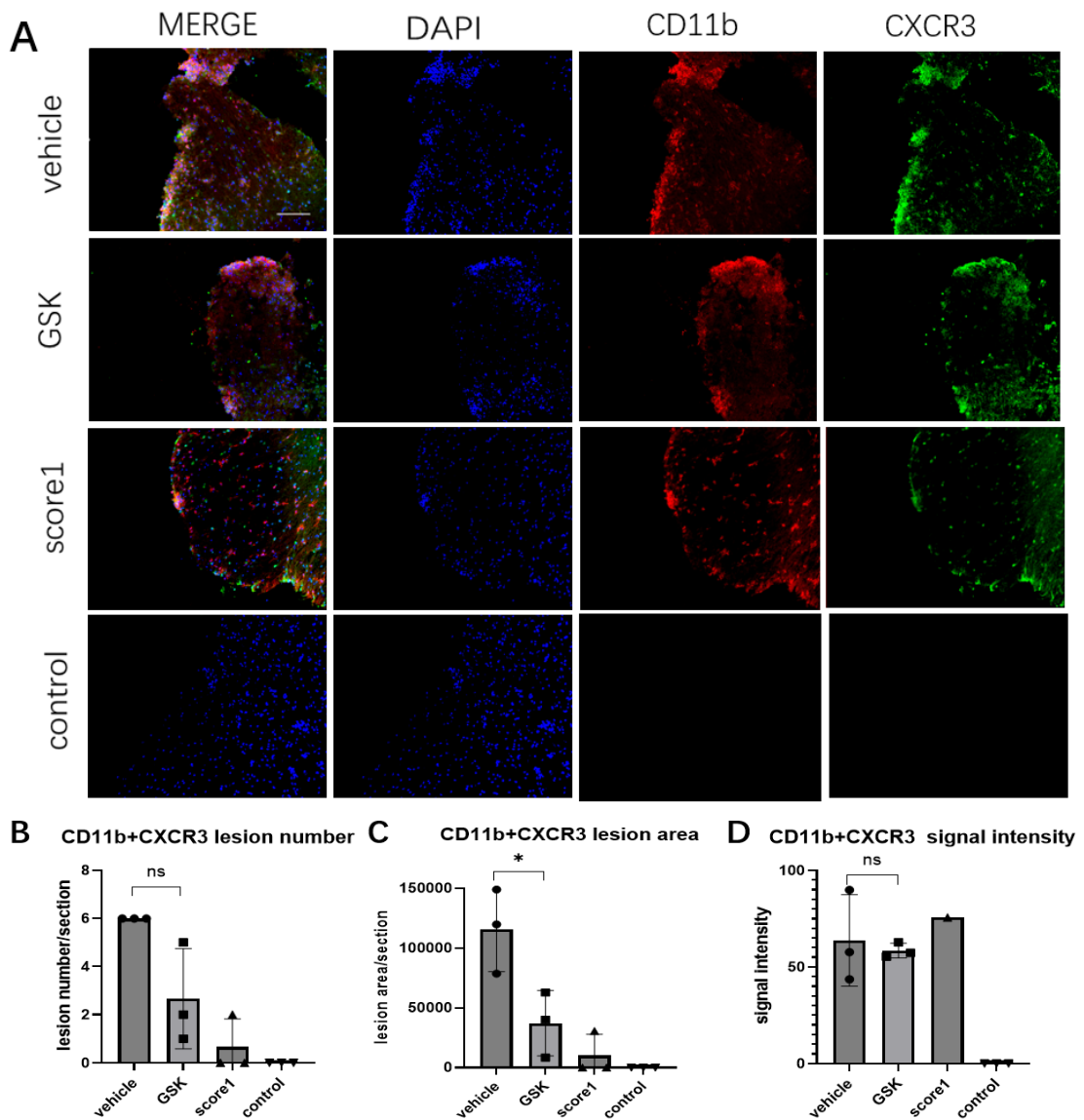


Figure 3.2: CD11b + CXCR3 signal showed the highest in vehicle and reduced in GSK, score1 and control (scale bar=100  $\mu$ m). (A) Spinal cord slides were stained with CD11b, CXCR3 and DAPI. The 20x images of lesion sites were analyzed by Keyence microscopy. Quantification of lesions in vehicle, GSK, score1 and control are shown in (B-D). (B) Lesion number of each spinal cord section. (C) Lesion area of each spinal cord section. (D) Signal intensity of the lesion sites. Data were analyzed by student's t-test and are expressed as mean  $\pm$  standard error

counted when we collected data, whereas lesion area, which is a more reasonable way to reflect disease progression, showed significant difference between vehicle and GSK (vehicle=122670 $\pm$ 11308 vs. GSK=36830 $\pm$ 14368,  $P < 0.05$ ).

Similarly, in CD11b and CXCR3 staining, lesion number and area accumulated from control, score1 and GSK to vehicle. Also, the lesion number did not show

significant difference for the same reason, but lesion area did (lesion number: vehicle =  $6.00 \pm 0.00$  vs. GSK =  $2.66 \pm 1.20$ ,  $P > 0.05$ ; lesion area: vehicle =  $115895 \pm 20349$  vs. GSK =  $37222 \pm 15803$ ,  $P < 0.05$ ). In addition, no reduction was observed in the signal intensity (vehicle =  $63.73 \pm 13.70$ , GSK =  $58.50 \pm 2.21$ , score1 =  $75.66 \pm 0.00$ , control =  $0.00 \pm 0.00$ ,  $P > 0.05$ ) (Figure 3.2B-D).

Therefore, these results confirmed that CCR5 and CXCR3 accumulated as the disease progressed, which correspond with the data we got from flow cytometry, and demonstrated that RIP1 inhibitor is able to protect EAE spinal cord and prevent the disease progression.

### 3.2. CCR5 and CXCR3 signal are outside nucleus in lesion and greatly reduce in uninjured area.

In the prior study to confirm how CCR5 and CXCR3 signal change in vehicle-GSK-score1-control spinal cord slides, we found that the signal showed up on the surface of the lesion cells. To further determine where the signal locate, we observed the sections with high magnification. Both CCR5 and CXCR3, which are receptors of CCL5 and CXCL10, appeared outside the nucleus in the lesions and the signal of both of them decreased or even disappeared in the uninjured area compared with lesion sites (Figure 3.3 A, B).

Furthermore, we did CCL5 staining with CD11b. Unlike CCR5 and CXCR3, CCL5 clearly stained cell bodies and overlapped with DAPI and CD11b, which demonstrated that these cells secreted cytokines CCL5 themselves, and CCL5 signal

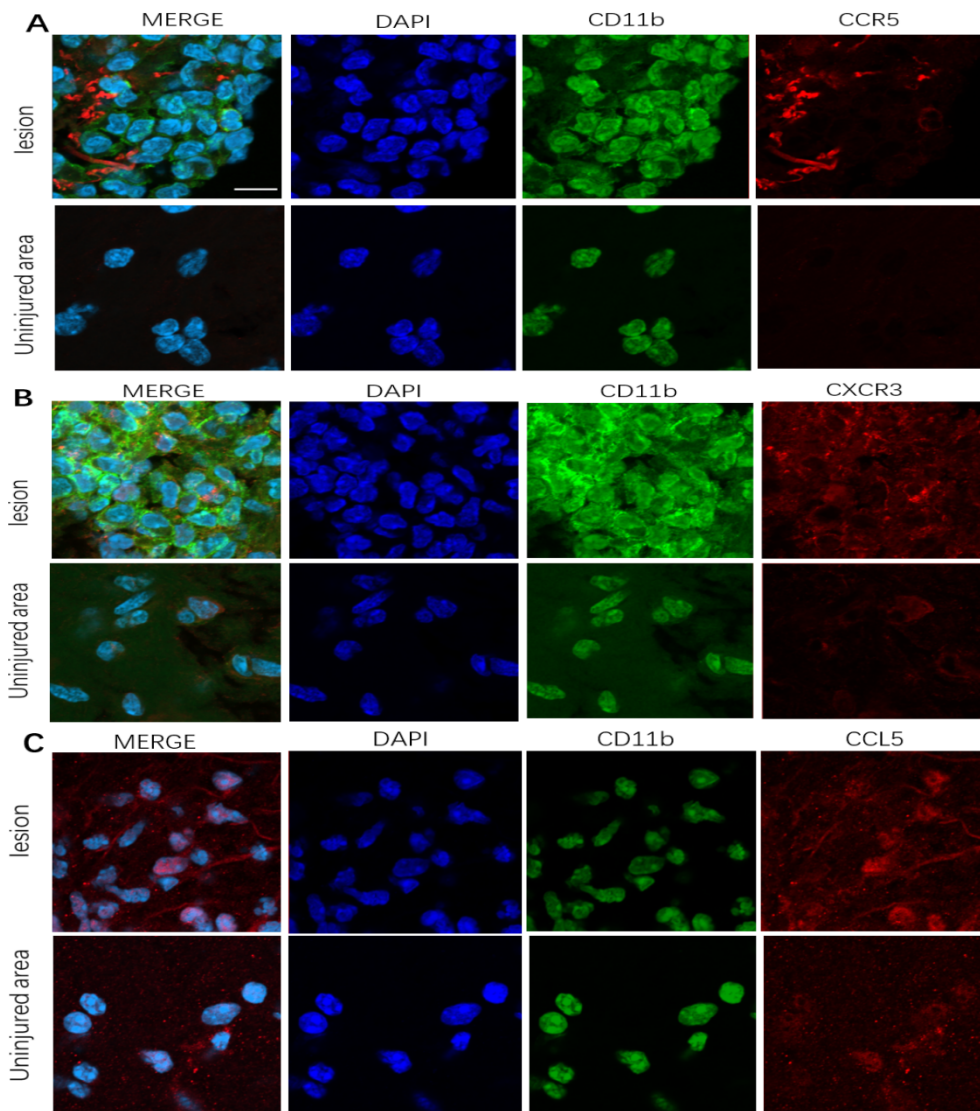


Figure 3.3: High magnification images of CCR5, CXCR3 and CCL5 in lesion and uninjured area. In lesions, CCR5 and CXCR3 were outside the nucleus, whereas CCL5 co-located with DAPI and CD11b. In uninjured area, CCR5 and CXCR3 signal almost disappeared, while CCL5 still existed (scale bar=10  $\mu$ m). (A) CCR5 co-stained with CD11b and DAPI. (B) CXCR3 co-stained with CD11b and DAPI. (C) CCL5 co-stained with CD11b and DAPI.

still existed in the uninjured area, suggesting that some cells in uninjured area also produced CCL5 (Figure 3.3 C)

### 3.3. Majority of the cells in lesion are macrophage, and in uninjured area are microglia.

To further investigate which kind of cells exist in the lesion and uninjured area of EAE mice spinal cord, we did co-staining of CD45 and Iba-1, which is the marker of

macrophage and microglia, on vehicle spinal cord slides, and 5 images of lesion sites and 5 images of uninjured area were taken.

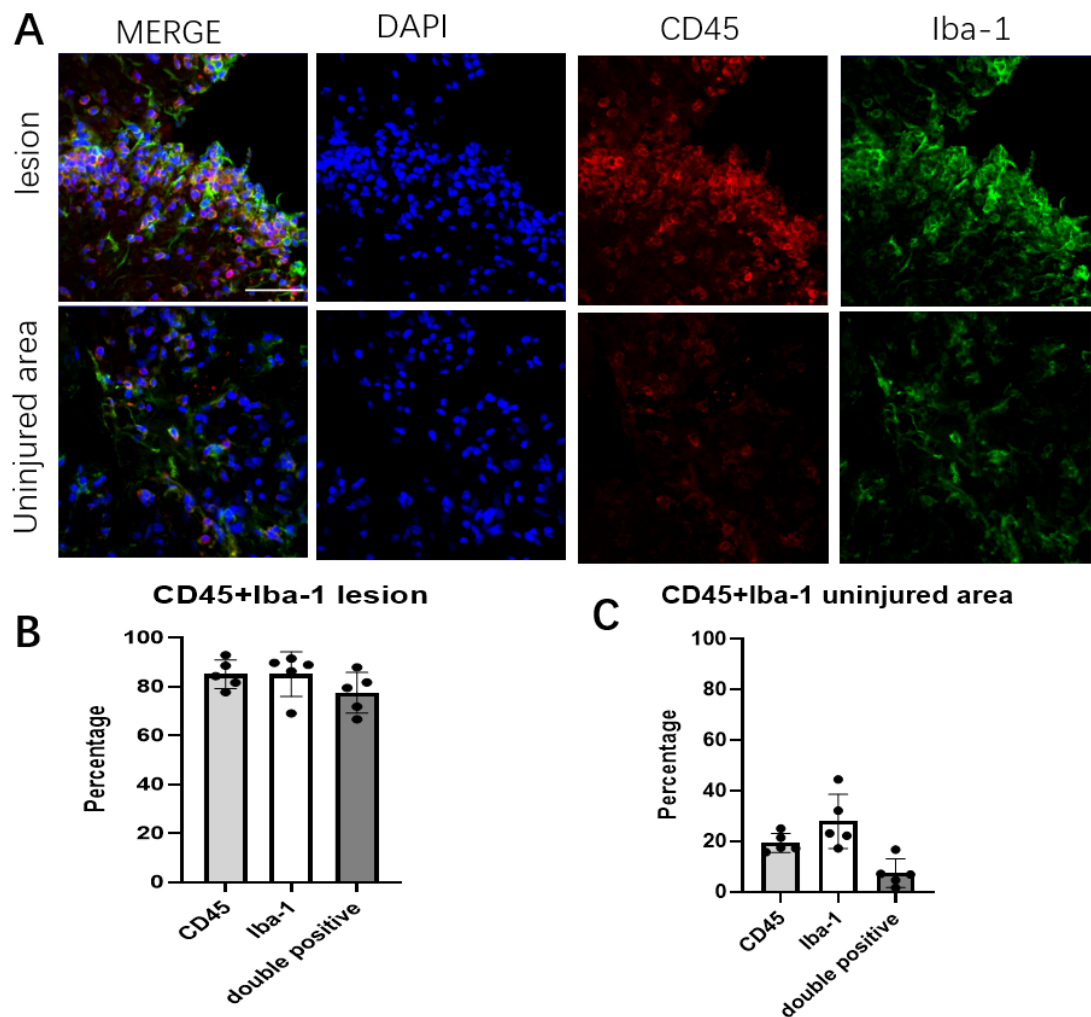


Figure 3.4: Most of cells in lesion are CD45 and Iba-1 double positive cells, whereas in uninjured area few of CD45 and Iba-1 co-located (scale bar=50  $\mu$ m). (A) High magnification image of CD45 and Iba-1 in lesion and uninjured area. Percentage of CD45 cells, Iba-1 cells and double positive cells in the whole population in lesion (B) and in uninjured area (C). Image of five lesions and five uninjured area were collected, and cell number was counted on Image J. Data are expressed as mean $\pm$ standard error.

After counting number of cells in DAPI, CD45 and Iba-1 from these five sets of images, we found that in CD45 and Iba-1 co-staining, there were 85.01% of cells in DAPI were CD45 positive and 85.04% were Iba-1 positive cells, and most of them were double positive (77.49%) in lesions (Figure 3.4 B). Meanwhile, in uninjured area, both the percentage of CD45 and Iba-1 positive cells decreased dramatically, to 19.37% and 27.84%, and there were only 7.38% cells were double positive (Figure 3.4

C).

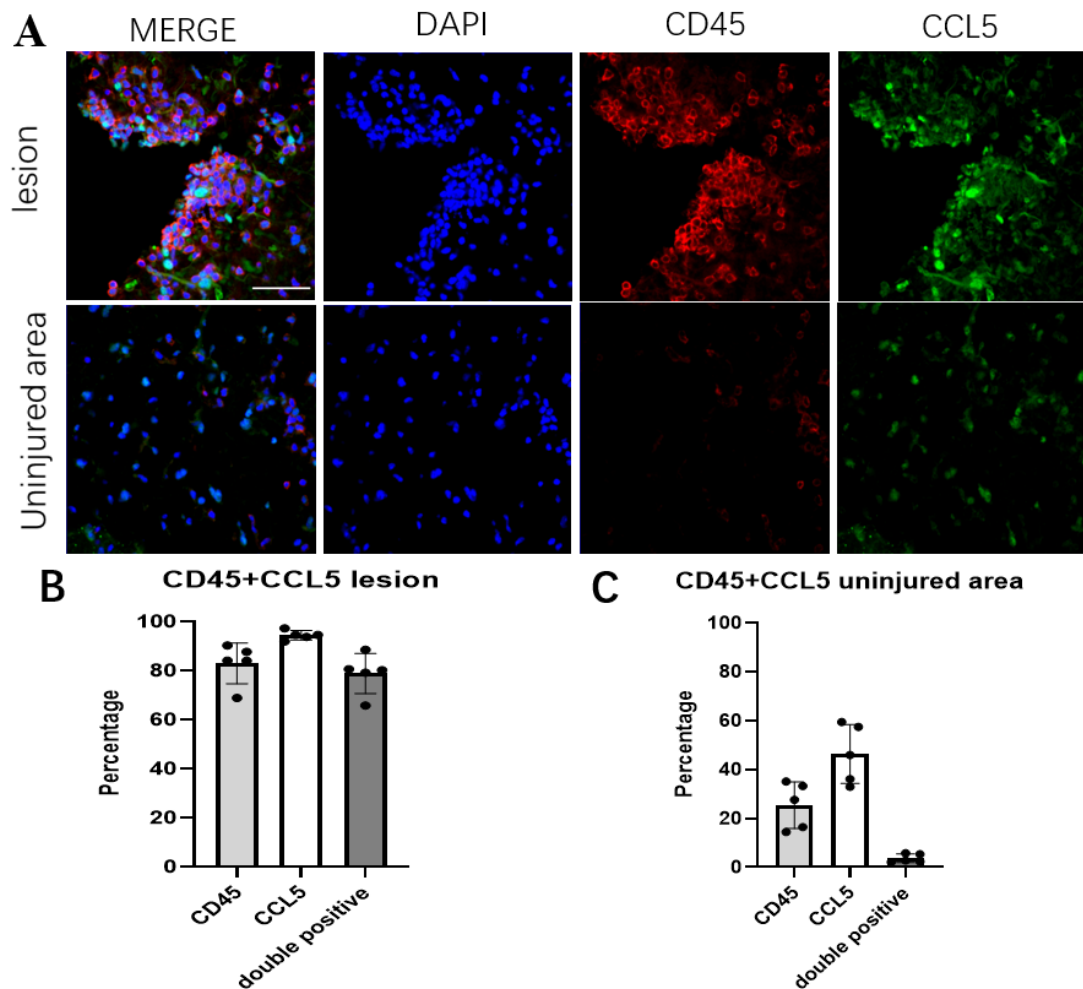


Figure 3.5: CD45 and CCL5 double positive make up the majority of cells in lesion, while in uninjured area there is almost none of double positive cells (scale bar=50  $\mu$ m). (A) High magnification image of CD45 and CCL5 in lesion and uninjured area. Percentage of CD45 cells, CCL5 cells and double positive cells in the whole population in lesion. (B) and in uninjured area (C). Image of five lesions and five uninjured areas were collected, and cell number was counted on Image J. Data are expressed as mean $\pm$ standard error.

Meanwhile, the data from our previous flow cytometry demonstrated that macrophage expressed higher level of CD45 while microglia expressed lower level. Taken together these findings, we found that most of the cells in lesions are macrophage, and in uninjured area are microglia.

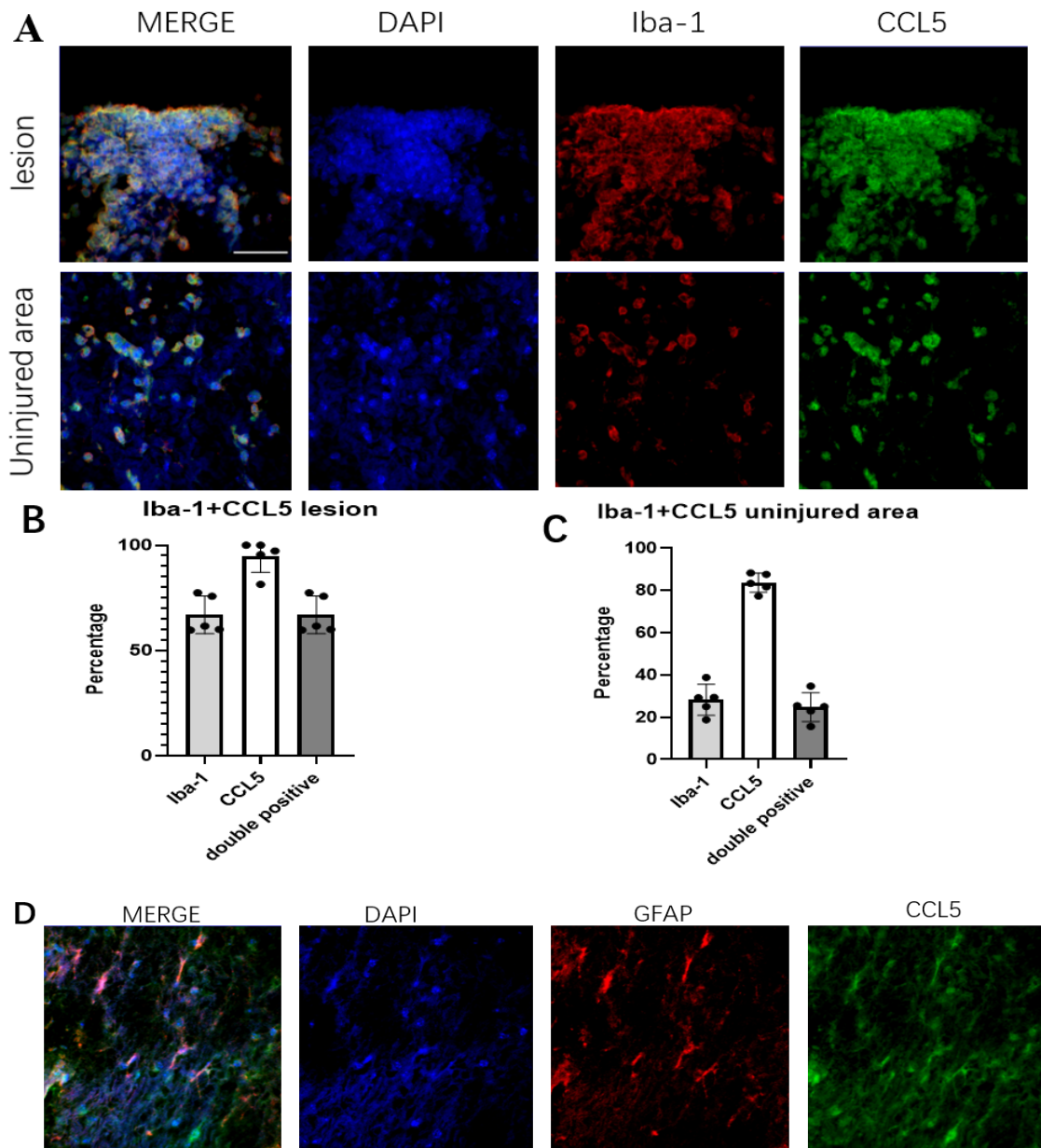


Figure 3.6: All the Iba-1 cells were CCL5 positive in lesions, while in uninjured area a few Iba-1 cells did not secrete CCL5 (scale bar=50  $\mu$ m). (A) High magnification image of CD45 and CCL5 in lesion and uninjured area. Percentage of Iba-1 cells, CCL5 cells and double positive cells in the whole population in lesions. (B) and in uninjured area (C). (D) GFAP was stained with CCL6. Image of five lesions and five uninjured area were collected, and cell number was counted on Image J. Data are expressed as mean  $\pm$  standard error.

### 3.4. Both macrophage and microglia produce CCL5.

After knowing that macrophage and microglia are in the EAE mice spinal cord, we examined whether they produced CCL5, by staining CD45 with CCL5, and Iba-1 with CCL5.

In CD45 and CCL5 staining, percentage of CCL5 was 94.55% in lesion which was higher than CD45(83.08%), and 78.96% cells in lesion were double positive, indicating that same as CD45+ Iba-1 staining, some cells were only stained with CD45 without CCL5. In uninjured area, CCL5 cells (46.37%) were almost double of CD45(25.42%), but only 3.69% was double positive, suggesting that the microglia here were less activated. Further, different from CD45+CCL5 staining, all the Iba-1 cells (66.93%) were overlap with CCL5 (94.85%) in lesions. And in uninjured area, a few Iba-1 cells were not CCL5 positive. These results suggested that both microglia and macrophage secretes CCL5 cytokine.

To examine which cell type also produce CCL5 in uninjured area, we tried to stained GFAP, the marker of astrocytes, with CCL5. The images showed that some astrocytes were CCL5 positive. Thus, not only microglia but also astrocytes secret CCL5 in uninjured area in EAE spinal cord.

#### 3.4. Collaboration

All the figures were finished by Jiya Hao.

## Chapter 4: Discussion

### 4.1. RIPK1 inhibitor affects the recruitment of CCR5<sup>+</sup> and CXCR3<sup>+</sup> cells to lesion.

In our previous study, we collected microglia and astrocyte from spinal cord of vehicle, GSK, score1 and control EAE mice. After the detection of genes and chemokines expression in these cells, we found that CCL5 and CXCL10 were upregulated in cells from vehicle sample and downregulated in GSK and score1. CCL5 and CXCL10 are critical proinflammatory chemokine. CCR5 is one of CCL5 receptor and their combination serves a role in inflammatory responses, as well as inducing the adhesion and migration of different T cell subsets in immune responses (Marques, Guabiraba et al. 2013, Zeng, Lan et al. 2022). CXCL10 is able to attract CD8<sup>+</sup> and CD4<sup>+</sup> effector T cells to the sites of inflammation, and CXCR3 is its receptor (Karin and Razon 2018).

Here, to confirm that result, we stained CCR5 and CXCR3 respectively with CD11b, which is a marker of myeloid cells, on spinal cord slides of four conditions. We evaluated the progression of the disease by analyzing the number, area, and signal intensity of lesions in four sets of spinal cord slides, and the results showed that both lesion number and area decreased in score1 and GSK treated groups compared with vehicle. Therefore, RIPK1 inhibitor GSK is able to prevent the recruitment of CCR5<sup>+</sup> and CXCR3<sup>+</sup> cells to lesion, and attenuate disease progression in EAE mice model in a manner that signal intensity in lesions is not changed. However, after we observed the spinal cord sections under high magnification lens, we found that CCR5 and CXCR3 signal appeared on the cell surface, while CCL5 was inside, so in the following experiment we used CCL5 as the marker.

#### 4.2. Cell composition in EAE spinal cord.

Though we proved that RIPK1 inhibitor GSK indeed stopped disease progressing, the underlying mechanism remains unclear. To figure out how GSK is working, it is important to know what happens in multiple sclerosis. Thus, only on vehicle samples we stained CD45 with Iba-1, which is the marker for microglia and macrophage. The results showed that in lesions, almost all the cells were CD45 and Iba-1 double positive, while in uninjured area the percentage of double positive cells decreased. Combined with our previous flow cytometry results, which revealed that macrophage expressed higher level of CD45 while microglia expressed lower level, we demonstrated that the cells in lesion are macrophage and in uninjured area the cells are microglia.

To figure out which kind of cell produce CCL5 in EAE mice spinal cord, we operated CD45+CCL5 and Iba-1+CCL5 staining. Our results showed that all the cells that expressed Iba-1 produce CCL5 in lesions, while in uninjured area some Iba-1 cells did not express CCL5. From this, it appears macrophage and microglia both expressed CCL5. As not all Iba-1 cells in uninjured area expressed CCL5, we further explored which kind of cell type also produce CCL5 in uninjured area. A previous study demonstrated that RIPK1 kinase activation in microglia and astrocytes induces a detrimental neuroinflammatory program that contributes to the neurodegenerative environment in progressive MS (Zelic, Pontarelli et al. 2021), so we tried to stain GFAP, the marker of astrocyte, with CCL5. We found that astrocytes also produce CCL5 in uninjured area. Moreover, in CD45+CCL5 staining, the rate of double positive cells decreased markedly in uninjured area compared with lesion, we thought this may due to the less activated microglia in uninjured area.

### 4.3. limitations and Further studies

In this paper two kinds of staining methods were adopted. Except regular IHC frozen section staining protocol, we also used Multiplex IHC (Opal 4 Color Manual IHC Kits), as Iba-1, GFAP and CCL5 are all anti-rabbit antibodies. By using this kit, the background of image is higher than the regular IHC protocol.

After we have found that macrophage, microglia and astrocytes expressed CCL5 in EAE mouse spinal cord, we will stain both Iba-1 and GFAP with CCL5 on vehicle, GSK, score1 and control, and evaluate the difference between these four conditions. In this way we would possibly figure out the mechanism of how RIPK1 inhibitor GSK prevent disease progression and protect EAE mice. Further, we would also measure whether RIPK2 inhibitor has the same effect in EAE as RIPK1 inhibitor. We will generate four group of EAE mice: WT vehicle, WT treated by RIPK2 inhibitor, RIPK2 KO vehicle and WT control, and stain flouromyelin and CD45 on spinal cord slides.

## Chapter 5: Appendix – Mouse EAE scoring guide

Typically, EAE is scored on scale 0 to 5. Most researchers also give mice “in between” scores (i.e. 0.5, 1.5, 2.5) when the clinical picture lies between two defined scores.

Score	Clinical observations
0.0	No obvious changes in motor function. When picked up by base of tail, the tail has tension and is erect. Hind legs are usually spread apart. When the mouse is walking, there is no gait or head tilting.
1.0	Limp tail. When picked up by base of tail, instead of being erect, the whole tail drapes over finger. Hind legs are usually spread apart. No signs of tail movement are observed.
2.0	Limp tail and weakness of hind legs. When picked up by base of tail, the legs are not spread apart, but held closer together. When the mouse is observed walking, it has a clearly apparent wobbly walk. One foot may have toes dragging, but the other leg has no apparent inhibitions of movement.
3.0	Limp tail and complete paralysis of hind legs (most common). Or limp tail and almost complete paralysis of hind legs. One or both hind legs are able to peddle, but neither hind leg is able to move forward of the hind hip.
4.0	Limp tail and complete hind leg and partial front leg paralysis. Mouse is minimally moving around the cage but appears alert and feeding.
5.0	Mouse is spontaneously rolling in the cage. Or mouse is found dead due to paralysis.

## Chapter 6: Bibliography

- Aldinucci, D. and A. Colombatti (2014). "The inflammatory chemokine CCL5 and cancer progression." Mediators Inflamm **2014**: 292376.
- Bertheloot, D., E. Latz and B. S. Franklin (2021). "Necroptosis, pyroptosis and apoptosis: an intricate game of cell death." Cell Mol Immunol **18**(5): 1106-1121.
- Compston, A. and A. Coles (2008). "Multiple sclerosis." Lancet **372**(9648): 1502-1517.
- Constantinescu, C. S., N. Farooqi, K. O'Brien and B. Gran (2011). "Experimental autoimmune encephalomyelitis (EAE) as a model for multiple sclerosis (MS)." Br J Pharmacol **164**(4): 1079-1106.
- Degterev, A., Z. Huang, M. Boyce, Y. Li, P. Jagtap, N. Mizushima, G. D. Cuny, T. J. Mitchison, M. A. Moskowitz and J. Yuan (2005). "Chemical inhibitor of nonapoptotic cell death with therapeutic potential for ischemic brain injury." Nat Chem Biol **1**(2): 112-119.
- Degterev, A., D. Ofengeim and J. Yuan (2019). "Targeting RIPK1 for the treatment of human diseases." Proc Natl Acad Sci U S A **116**(20): 9714-9722.
- Dobson, R. and G. Giovannoni (2019). "Multiple sclerosis - a review." Eur J Neurol **26**(1): 27-40.
- Dulamea, A. O. (2017). "Role of Oligodendrocyte Dysfunction in Demyelination, Remyelination and Neurodegeneration in Multiple Sclerosis." Adv Exp Med Biol **958**: 91-127.
- Garg, N. and T. W. Smith (2015). "An update on immunopathogenesis, diagnosis, and treatment of multiple sclerosis." Brain Behav **5**(9): e00362.
- Guerrero-Garcia, J. J. (2020). "The role of astrocytes in multiple sclerosis pathogenesis." Neurologia (Engl Ed) **35**(6): 400-408.
- Harris, P. A., N. Faucher, N. George, P. M. Eidam, B. W. King, G. V. White, N. A. Anderson, D. Bandyopadhyay, A. M. Beal, V. Beneton, S. B. Berger, N. Campobasso, S. Campos, C. A. Capriotti, J. A. Cox, A. Daugan, F. Donche, M. H. Fouchet, J. N. Finger, B. Geddes, P. J. Gough, P. Grondin, B. L. Hoffman, S. J. Hoffman, S. E. Hutchinson, J. U. Jeong, E. Jigorel, P. Lamoureux, L. K. Leister, J. D. Lich, M. K. Mahajan, J. Meslamani, J. E. Mosley, R. Nagilla, P. M. Nassau, S. L. Ng, M. T. Ouellette, K. K. Pasikanti, F. Potvain, M. A. Reilly, E. J. Rivera, S. Sautet, M. C. Schaeffer, C. A. Schon, H. Sun, J. H. Thorpe, R. D. Totoritis, P. Ward, N. Wellaway, D. D. Wisnoski, J. M. Woolven, J. Bertin and R. W. Marquis (2019). "Discovery and Lead-Optimization of 4,5-Dihydropyrazoles as Mono-Kinase Selective, Orally Bioavailable and Efficacious Inhibitors of Receptor Interacting Protein 1 (RIP1) Kinase." J Med Chem **62**(10): 5096-5110.
- Hinrichs, A. C., S. L. M. Blokland, A. A. Kruize, F. P. J. Lafeber, H. L. Leavis and J. A. G. van Roon (2022). "CCL5 Release by CCR9+ CD8 T Cells: A Potential Contributor to Immunopathology of Primary Sjogren's Syndrome." Front Immunol **13**: 887972.
- Huang, R., L. Guo, M. Gao, J. Li and S. Xiang (2021). "Research Trends and Regulation of CCL5 in Prostate Cancer." Onco Targets Ther **14**: 1417-1427.
- Inglese, M. (2006). "Multiple sclerosis: new insights and trends." AJNR Am J Neuroradiol **27**(5): 954-957.
- International Multiple Sclerosis Genetics, C., C. Wellcome Trust Case Control, S. Sawcer, G. Hellenthal, M. Pirinen, C. C. Spencer, N. A. Patsopoulos, L. Moutsianas, A. Dilthey, Z. Su, C. Freeman, S. E. Hunt, S. Edkins, E. Gray, D. R.

- Booth, S. C. Potter, A. Goris, G. Band, A. B. Oturai, A. Strange, J. Saarela, C. Bellenguez, B. Fontaine, M. Gillman, B. Hemmer, R. Gwilliam, F. Zipp, A. Jayakumar, R. Martin, S. Leslie, S. Hawkins, E. Giannoulatou, S. D'Alfonso, H. Blackburn, F. Martinelli Boneschi, J. Liddle, H. F. Harbo, M. L. Perez, A. Spurkland, M. J. Waller, M. P. Mycko, M. Ricketts, M. Comabella, N. Hammond, I. Kockum, O. T. McCann, M. Ban, P. Whittaker, A. Kempainen, P. Weston, C. Hawkins, S. Widaa, J. Zajicek, S. Dronov, N. Robertson, S. J. Bumpstead, L. F. Barcellos, R. Ravindrarajah, R. Abraham, L. Alfredsson, K. Ardlie, C. Aubin, A. Baker, K. Baker, S. E. Baranzini, L. Bergamaschi, R. Bergamaschi, A. Bernstein, A. Berthele, M. Boggild, J. P. Bradfield, D. Brassat, S. A. Broadley, D. Buck, H. Butzkueven, R. Capra, W. M. Carroll, P. Cavalla, E. G. Celius, S. Cepok, R. Chiavacci, F. Clerget-Darpoux, K. Clysters, G. Comi, M. Cossburn, I. Cournu-Rebeix, M. B. Cox, W. Cozen, B. A. Cree, A. H. Cross, D. Cusi, M. J. Daly, E. Davis, P. I. de Bakker, M. Debouverie, B. D'Hooghe M, K. Dixon, R. Dobosi, B. Dubois, D. Ellinghaus, I. Elovaara, F. Esposito, C. Fontenille, S. Foote, A. Franke, D. Galimberti, A. Ghezzi, J. Glessner, R. Gomez, O. Gout, C. Graham, S. F. Grant, F. R. Guerini, H. Hakonarson, P. Hall, A. Hamsten, H. P. Hartung, R. N. Heard, S. Heath, J. Hobart, M. Hoshi, C. Infante-Duarte, G. Ingram, W. Ingram, T. Islam, M. Jagodic, M. Kabesch, A. G. Kermod, T. J. Kilpatrick, C. Kim, N. Klopp, K. Koivisto, M. Larsson, M. Lathrop, J. S. Lechner-Scott, M. A. Leone, V. Leppa, U. Liljedahl, I. L. Bomfim, R. R. Lincoln, J. Link, J. Liu, A. R. Lorentzen, S. Lupoli, F. Macciardi, T. Mack, M. Marriott, V. Martinelli, D. Mason, J. L. McCauley, F. Mentch, I. L. Mero, T. Mihalova, X. Montalban, J. Mottershead, K. M. Myhr, P. Naldi, W. Ollier, A. Page, A. Palotie, J. Pelletier, L. Piccio, T. Pickersgill, F. Piehl, S. Pobywajlo, H. L. Quach, P. P. Ramsay, M. Reunanen, R. Reynolds, J. D. Rioux, M. Rodegher, S. Roesner, J. P. Rubio, I. M. Ruckert, M. Salvetti, E. Salvi, A. Santaniello, C. A. Schaefer, S. Schreiber, C. Schulze, R. J. Scott, F. Sellebjerg, K. W. Selmaj, D. Sexton, L. Shen, B. Simms-Acuna, S. Skidmore, P. M. Sleiman, C. Smestad, P. S. Sorensen, H. B. Sondergaard, J. Stankovich, R. C. Strange, A. M. Sulonen, E. Sundqvist, A. C. Syvanen, F. Taddeo, B. Taylor, J. M. Blackwell, P. Tienari, E. Bramon, A. Tourbah, M. A. Brown, E. Tronczynska, J. P. Casas, N. Tubridy, A. Corvin, J. Vickery, J. Jankowski, P. Villoslada, H. S. Markus, K. Wang, C. G. Mathew, J. Wason, C. N. Palmer, H. E. Wichmann, R. Plomin, E. Willoughby, A. Rautanen, J. Winkelmann, M. Wittig, R. C. Trembath, J. Yaouanq, A. C. Viswanathan, H. Zhang, N. W. Wood, R. Zuvich, P. Deloukas, C. Langford, A. Duncanson, J. R. Oksenberg, M. A. Pericak-Vance, J. L. Haines, T. Olsson, J. Hillert, A. J. Ivinson, P. L. De Jager, L. Peltonen, G. J. Stewart, D. A. Hafler, S. L. Hauser, G. McVean, P. Donnelly and A. Compston (2011). "Genetic risk and a primary role for cell-mediated immune mechanisms in multiple sclerosis." *Nature* **476**(7359): 214-219.
- Jakel, S., E. Agirre, A. Mendanha Falcao, D. van Bruggen, K. W. Lee, I. Knuesel, D. Malhotra, C. Ffrench-Constant, A. Williams and G. Castelo-Branco (2019). "Altered human oligodendrocyte heterogeneity in multiple sclerosis." *Nature* **566**(7745): 543-547.
- Kamma, E., W. Lasisi, C. Libner, H. S. Ng and J. R. Plemel (2022). "Central nervous system macrophages in progressive multiple sclerosis: relationship to neurodegeneration and therapeutics." *J Neuroinflammation* **19**(1): 45.
- Karin, N. and H. Razon (2018). "Chemokines beyond chemo-attraction: CXCL10 and its significant role in cancer and autoimmunity." *Cytokine* **109**: 24-28.

- Karunakaran, D., M. A. Nguyen, M. Geoffrion, D. Vreeken, Z. Lister, H. S. Cheng, N. Otte, P. Essebier, H. Wyatt, J. W. Kandiah, R. Jung, F. J. Alenghat, A. Mompeon, R. Lee, C. Pan, E. Gordon, A. Rasheed, A. J. Lusic, P. Liu, L. P. Matic, U. Hedin, J. E. Fish, L. Guo, F. Kolodgie, R. Virmani, J. M. van Gils and K. J. Rayner (2021). "RIPK1 Expression Associates With Inflammation in Early Atherosclerosis in Humans and Can Be Therapeutically Silenced to Reduce NF-kappaB Activation and Atherogenesis in Mice." *Circulation* **143**(2): 163-177.
- Kim, S. J. and J. Li (2013). "Caspase blockade induces RIP3-mediated programmed necrosis in Toll-like receptor-activated microglia." *Cell Death Dis* **4**(7): e716.
- Kranjc, M. K., M. Novak, R. G. Pestell and T. T. Lah (2019). "Cytokine CCL5 and receptor CCR5 axis in glioblastoma multiforme." *Radiol Oncol* **53**(4): 397-406.
- Lawrence, T. (2009). "The nuclear factor NF-kappaB pathway in inflammation." *Cold Spring Harb Perspect Biol* **1**(6): a001651.
- Marques, R. E., R. Guabiraba, R. C. Russo and M. M. Teixeira (2013). "Targeting CCL5 in inflammation." *Expert Opin Ther Targets* **17**(12): 1439-1460.
- Mifflin, L., D. Ofengeim and J. Yuan (2020). "Receptor-interacting protein kinase 1 (RIPK1) as a therapeutic target." *Nat Rev Drug Discov* **19**(8): 553-571.
- Nicholas, R. and W. Rashid (2013). "Multiple sclerosis." *Am Fam Physician* **87**(10): 712-714.
- Ofengeim, D., Y. Ito, A. Najafov, Y. Zhang, B. Shan, J. P. DeWitt, J. Ye, X. Zhang, A. Chang, H. Vakifahmetoglu-Norberg, J. Geng, B. Py, W. Zhou, P. Amin, J. Berlink Lima, C. Qi, Q. Yu, B. Trapp and J. Yuan (2015). "Activation of necroptosis in multiple sclerosis." *Cell Rep* **10**(11): 1836-1849.
- Pegoretti, V., W. Baron, J. D. Laman and U. L. M. Eisel (2018). "Selective Modulation of TNF-TNFRs Signaling: Insights for Multiple Sclerosis Treatment." *Front Immunol* **9**: 925.
- Ponath, G., M. R. Lincoln, M. Levine-Ritterman, C. Park, S. Dahlawi, M. Mubarak, T. Sumida, L. Airas, S. Zhang, C. Isitan, T. D. Nguyen, C. S. Raine, D. A. Hafler and D. Pitt (2018). "Enhanced astrocyte responses are driven by a genetic risk allele associated with multiple sclerosis." *Nat Commun* **9**(1): 5337.
- Robinson, A. P., C. T. Harp, A. Noronha and S. D. Miller (2014). "The experimental autoimmune encephalomyelitis (EAE) model of MS: utility for understanding disease pathophysiology and treatment." *Handb Clin Neurol* **122**: 173-189.
- Selter, R. C. and B. Hemmer (2013). "Update on immunopathogenesis and immunotherapy in multiple sclerosis." *Immunotargets Ther* **2**: 21-30.
- Shan, B., H. Pan, A. Najafov and J. Yuan (2018). "Necroptosis in development and diseases." *Genes Dev* **32**(5-6): 327-340.
- Srinivasan, K., B. A. Friedman, J. L. Larson, B. E. Lauffer, L. D. Goldstein, L. L. Appling, J. Borneo, C. Poon, T. Ho, F. Cai, P. Steiner, M. P. van der Brug, Z. Modrusan, J. S. Kaminker and D. V. Hansen (2016). "Untangling the brain's neuroinflammatory and neurodegenerative transcriptional responses." *Nat Commun* **7**: 11295.
- Yamout, B. I. and R. Alroughani (2018). "Multiple Sclerosis." *Semin Neurol* **38**(2): 212-225.
- Yeung, M. S. Y., M. Djelloul, E. Steiner, S. Bernard, M. Salehpour, G. Possnert, L. Brundin and J. Frisen (2019). "Dynamics of oligodendrocyte generation in multiple sclerosis." *Nature* **566**(7745): 538-542.
- Yoshikawa, M., M. Saitoh, T. Katoh, T. Seki, S. V. Bigi, Y. Shimizu, T. Ishii, T. Okai, M. Kuno, H. Hattori, E. Watanabe, K. S. Saikatendu, H. Zou, M. Nakakariya, T. Tatamiya, Y. Nakada and T. Yogo (2018). "Discovery of 7-Oxo-2,4,5,7-

- tetrahydro-6 H-pyrazolo[3,4- c]pyridine Derivatives as Potent, Orally Available, and Brain-Penetrating Receptor Interacting Protein 1 (RIP1) Kinase Inhibitors: Analysis of Structure-Kinetic Relationships." J Med Chem **61**(6): 2384-2409.
- Yu, Z., N. Jiang, W. Su and Y. Zhuo (2021). "Necroptosis: A Novel Pathway in Neuroinflammation." Front Pharmacol **12**: 701564.
- Yuan, J., P. Amin and D. Ofengeim (2019). "Necroptosis and RIPK1-mediated neuroinflammation in CNS diseases." Nat Rev Neurosci **20**(1): 19-33.
- Zelic, M., F. Pontarelli, L. Woodworth, C. Zhu, A. Mahan, Y. Ren, M. LaMorte, R. Gruber, A. Keane, P. Loring, L. Guo, T. H. Xia, B. Zhang, P. Orning, E. Lien, A. Degtarev, T. Hammond and D. Ofengeim (2021). "RIPK1 activation mediates neuroinflammation and disease progression in multiple sclerosis." Cell Rep **35**(6): 109112.
- Zeng, Z., T. Lan, Y. Wei and X. Wei (2022). "CCL5/CCR5 axis in human diseases and related treatments." Genes Dis **9**(1): 12-27.